Phase Behavior in Suspensions of Highly Charged Colloids

Andrey V. Brukhno,[†,‡] Torbjörn Åkesson,[§] and Bo Jönsson*[,§]

Self Organizing Molecular Systems (SOMS) Centre, School of Chemistry, Leeds University, Leeds LS2 9JT, United Kingdom, and Theoretical Chemistry, Chemical Center, POB 124, S-221 00 Lund, Sweden

Received: December 17, 2008; Revised Manuscript Received: March 11, 2009

Attractive interactions between like-charged aggregates (macromolecules, colloidal particles, or micelles) in solution due to electrostatic correlation effects are revisited. The associated phenomenon of phase separation in a colloidal solution of highly charged particles is directly observed in Monte Carlo simulations. We start with a simple, yet instructive, description of polarization effects in a "cloud" of counterions around a single charged aggregate and show how the ion−ion correlations can be mapped onto a classical analogue of the quantum-mechanical dispersion force. We then extend our treatment to the effective pair interaction between two such aggregates and provide an analysis of different interaction regimes, based on a simple coupling parameter. By computing the potential of mean force, we illustrate the physics behind the crossover between the regimes of pure repulsion and attraction with increasing counterion valency. Finally, we turn to semi grand *NpT* simulations of the corresponding bulk systems where mono- and multivalent ions can exchange with an external reservoir. Thus, the coagulation and phase separation phenomena, widely observed and used in real-life applications, are directly studied in these computer simulations.

Introduction

The stability of solutions that contain macromolecular aggregates, be they macromolecules, colloidal particles, or micelles, is determined by the net force acting between the aggregates. The effective force between highly charged colloids is usually dominated by long-ranged pairwise electrostatic interactions, which have a strong influence on the macroscopic properties displayed by the solution. A typical picture with a charged aggregate is that its surface accumulates small ions of opposite sign in its immediate neighborhood. As two such surfaces approach each other, their ionic atmospheres start to overlap, which often leads, for entropic reasons, to a strong long-range repulsion—a phenomenon commonly referred to as an electric double layer (EDL).[1,2] The traditional theoretical approach to the EDL problem is to disregard the structure of solvent and apply a mean-field approximation to interactions between ions. This classic theory developed by Derjaguin, Landau, Verwey, and Overbeek[3,4] (the DLVO theory), based on the Poisson−Boltzmann (PB) equation, has been very successful in describing a wide range of EDL phenomena. The most striking examples of the predictive capability of the PB equation have come from direct force measurements using a surface force apparatus.[5−7] Despite the wide (nearly universal) applicability of the PB equation, there exists a number of situations where the underlying theory apparently fails to describe experimental observations, not only quantitatively but also qualitatively.[8−16] One common feature of these exceptional circumstances is the presence of multivalent ions.

The breakdown of the PB theory can be ascribed to ionic correlation effects that are left out by the mean field approximation. The neglect of correlations is standard in approximate theoretical approaches to many-body problems and it is well-known that the accuracy of mean-field approximations deteriorates with increasing electrostatic coupling strength. This increased coupling can be brought about in different ways, for instance, by increasing the aggregate charge, lowering the temperature or the relative permittivity, or more abruptly, exchanging monovalent ions with multivalent ones.

Ion−ion correlation effects are naturally included in, for example, Monte Carlo simulations (with explicit treatment of ionic species),[17] advanced integral theories,[18,19] or the correlation corrected mean-field approach.[20] Numerous studies of correlations between ions in systems of various geometries (planar, cylindrical, spherical, etc.) show the same generic behavior. In particular, highly charged spherical aggregates have received a great deal of attention and also generated much debate with special emphasis on the range of the correlation attraction.[21−25] An extensive set of high quality simulation studies have been conducted by Linse and co-workers.[26−29] Their simulations show unequivocally how attractive forces, in the presence of multivalent counterions, start to dominate over the "normal" entropic double layer repulsion. This led the authors to predict the existence of a two-phase region in a certain parameter range. To our knowledge, the phase separation in colloidal suspensions due to ion−ion correlations has not yet been explicitly shown in a simulation. In this Article we present simulation results from a semi grand *NpT* ensemble, where one can directly observe the phase separation. The change from monovalent to divalent counterions is a dramatic step and we also show how one can make this transition in a gradual way by having a mix of competing mono- and multivalent counterions.

First, we consider a single charged aggregate (colloid) and its neutralizing counterions enclosed in a spherical cell. The classical polarizability of the cell serves as a simple starting point for describing the attraction induced by ion−ion correlations and how it can be related to the quantum mechanical dispersion force as introduced by London.[30] We then go on to study a two-colloid system demonstrating that the correlation attraction can actually dominate over the entropic counterion repulsion. In the final step we study a bulk system of charged

* Corresponding author. E-mail: bo.jonsson@teokem.lu.se.
† Leeds University.
‡ Earlier spelled as Andrei V. Broukhno. E-mail: abrukhno@gmail.com.
§ Chemical Center.

10.1021/jp811147v CCC: $40.75
Published on Web 04/15/2009

macro-aggregates and counterions of mixed valency. In these simulations we observe a crossover from supercritical phase behavior to phase separation depending on both the electrostatic coupling and the partitioning of small ionic species in the system.

Model and Simulation Techniques

We performed Monte Carlo (MC) simulations for three types of model systems:

•A single charged aggregate with its neutralizing counterions in a spherical cell.

•Two like-charged aggregates with their counterions in a spherical cell.

•A bulk solution of like-charged aggregates plus counterions, in a periodic cubic box.

The first two model systems were simulated in a canonical ensemble by use of the standard Metropolis algorithm.[31] The cell enclosing the aggregate(s) is taken to be spherical, and thus, the cell radius determines the aggregate concentration. That is, both the polarizability and the potential of mean force (POMF) calculated in these simulations are concentration dependent. It is a consequence of the zero salt concentration, and with a finite amount of salt, this peculiar behavior would disappear. The POMF's were obtained directly from the radial distribution functions, without any bias.

In all simulations we use the primitive model where water is treated as a uniform structureless medium with a dielectric permittivity $\epsilon_r = 78.7$ and a temperature $T = 298$ K. Aggregates and counterions are modeled as hard spheres with point charges, $Q_{agg} = Z_{agg}e$ and $q_{ci} = Z_{ci}e$, located in their centers, e being the elementary charge, $Z_{agg} < 0$ and $Z_{ci} > 0$. Thus, in the first case, with one aggregate in a spherical cell, the electrostatic interaction potential reads

$$U_{els} = \frac{e^2}{4\pi\epsilon_0\epsilon_r}\left[\sum_{i>j}^{N_{ci}} \frac{Z_{ci}^{\,2}}{r_{ij}} + \sum_{i}^{N_{ci}} \frac{Z_{ci}Z_{agg}}{r_{iA}}\right] \quad (1)$$

where r_{ij} and r_{iA} denote the distances between either two counterions (i and j) or a counterion (i) and the aggregate (A), and N_{ci} is the total number of counterions. Evidently, if any pair of particles happens to overlap, the total interaction becomes infinite and the attempted move is rejected. In the second case, with two charged aggregates, the interaction potential, with an obvious extension of the notation, is

$$U_{els} = \frac{e^2}{4\pi\epsilon_0\epsilon_r}\left[\sum_{i>j}^{N_{ci}} \frac{Z_{ci}^{\,2}}{r_{ij}} + \sum_{i}^{N_{ci}} \frac{Z_{ci}Z_{agg}}{r_{iA}} + \sum_{i}^{N_{ci}} \frac{Z_{ci}Z_{agg}}{r_{iB}} + \frac{Z_{agg}^{\,2}}{r_{AB}}\right] \quad (2)$$

In these two types of simulation the ion hard core radius of 2 Å and the aggregate radius of 10 Å are used.

In simulations of bulk systems we use a soft repulsive surface potential of Lennard-Jones type to improve efficiency of Monte Carlo moves at moderate to high aggregate densities. Namely, the core of small ionic species is treated as a soft repulsive particle whereas the aggregate softness is accounted for by use of a similar potential in the vicinity of its surface:

$$U_{surf} = \sum_{i>j}^{N_{ci}} u_{sr}(r_{ij}) + \sum_{i}^{N_{ci}}\sum_{A}^{N_{agg}} u_{sr}(r_{iA} - R_{agg}) + \sum_{A>B}^{N_{agg}} u_{sr}(r_{AB} - 2R_{agg}) \quad (3)$$

where $R_{agg} = 10$ Å is the aggregate radius and

$$u_{sr}(r) = \epsilon\left(\frac{d}{r}\right)^{12}$$

is the repulsive part of the Lennard-Jones pair potential. For simplicity we use the same values, $d = 4$ Å and $\epsilon = 1\ k_BT$, for all species, k_B being the Boltzmann constant. The conventional Ewald summation scheme (with the optimum choice of parameters)[32] is employed for calculating the electrostatic contribution, U_{els}, to the total interaction energy in the system,

$$U_{tot} = U_{els} + U_{surf} \quad (4)$$

Semi Grand Canonical Ensemble. The correlation effects due to replacement of monovalent counterions by competing divalent or trivalent ones are suitable for studying in the framework of semi grand ensembles.[32] To start with, in an ensemble where the number of aggregates, N_{agg}, temperature, T, and volume, V, are fixed, we periodically make attempts upon a mutation of a divalent (or trivalent) ion into monovalent ions, and vice versa. Apart from the obvious necessity to impose the overall electroneutrality, this stochastic mutation process is subject to the condition of keeping constant the chemical potential difference between counterions of the two valencies in question. In general, the procedure corresponds to simultaneous exchange of the ionic species with an (imaginary) reservoir containing infinitely diluted solution of appropriate salts. This way the composition of the solution under study can be varied while the system attains chemical equilibrium.

The characteristic thermodynamic (semi grand canonical) potential in this case is

$$\Xi(N_{agg},V,T,\Delta\mu_{ci}) = -k_BT \ln \mathcal{Z}(N_{agg},V,T,\Delta\mu_{ci}) \quad (5)$$

where the partition function, $\mathcal{Z}(N_{agg},V,T,\Delta\mu_{ci})$, can be obtained as follows. Consider a semi grand canonical ensemble where the chemical potentials, μ_1 and μ_z, of the ionic species of valencies ($\pm$)1 and $|z| > 1$ are fixed. The partition function in this ensemble is

$$\mathcal{Z}(N_{agg},V,T,\mu_1,\mu_z) = \sum_{N_1}\sum_{N_z} \exp\{\beta[\mu_1N_1 + \mu_zN_z]\} \times \frac{q_1^{N_1}q_z^{N_z}q_{agg}^{N_{agg}}}{N_1!N_z!N_{agg}!}V^N\int d\mathbf{u}^N \exp[-\beta U_{tot}(\mathbf{r}^N)] \quad (6)$$

where q_α is the kinetic factor for the corresponding species, $\beta = 1/k_BT$, $N = N_{agg} + N_1 + N_z$ is the total number of particles in the system and the configuration integral is expressed in terms of reduced coordinates, $\mathbf{u} = \mathbf{r}/L$, L being the simulation box length.

Now, due to the electroneutrality requirement, the composition of the system must be such that $|Z_{agg}|N_{agg} = N_1 + |z|N_z$. That is, the amounts of ionic species are not independent, and we can eliminate from eq 6 one of those; e.g., we can set $N_1 = |Z_{agg}|N_{agg} - |z|N_z$. Then, we switch from the double sum in eq 6 to the sum over N_z only, so as to obtain

$$\mathcal{Z}(N_{agg},V,T,\Delta\mu_{ci}) = \sum_{N_z} \exp\{\beta[\mu_1|Z_{agg}|N_{agg} + (\mu_z - |z|\mu_1)N_z]\} \times \frac{q_1^{(|Z_{agg}|N_{agg}-|z|N_z)}q_z^{N_z}q_{agg}^{N_{agg}}}{(|Z_{agg}|N_{agg} - |z|N_z)!N_z!N_{agg}!}V^N\int d\mathbf{u}^N \exp[-\beta U_{tot}(\mathbf{r}^N)] \quad (7)$$

Here we have introduced $\Delta\mu_{ci} = \mu_z - |z|\mu_1$. Finally, we also recognize that for our electrolyte systems eq 6 and eq 7 are equivalent, so that

$$\begin{aligned}\Xi(N_{agg},V,T,\Delta\mu_{ci}) &= A(\{N_\alpha\},V,T) - \mu_1 N_1 - \mu_z N_z \\ &= A(\{N_\alpha\},V,T) - \mu_1 |Z_{agg}| N_{agg} - \\ &\quad \Delta\mu_{ci} N_z = \mu_{agg} N_{agg} - pV\end{aligned} \quad (8)$$

Free Energy in a Semi Grand *NpT* Ensemble. A phase separation manifests itself in a bimodal shape of the Helmholtz free energy profile, $A(V) = U - TS$, which is due to a subtle interplay between the energetic and entropic contributions at different densities. The bimodality can though be more pronounced in the profile of a constrained Gibbs free energy as a function of V, $G_{NpT}(V) = A(V) + pV = -k_B T \ln[w(V;NpT)]$, where $w(V;NpT)$ is the volume probability density corresponding to a given pressure, $p = \text{const}$.[33,34] In the case of actual coexistence of two phases of different densities, $w(V;NpT)$ has two distinct maxima, and $G_{NpT}(V)$ exhibits two local minima of equal depth separated by a barrier. Alternatively, a similar bimodal behavior can be observed for the constrained grand potential as a function of composition, $\{N_\alpha\}$, $\Omega_{\{\mu_\alpha\},V,T}(\{N_\alpha\}) = A(V) - \Sigma\mu_\alpha N_\alpha = -k_B T \ln[w(\{N_\alpha\};\{\mu_\alpha\},V,T)]$, where the minima occur at different amounts of species present in the system.[35]

In general, the latter ansatz may seem more natural for multicomponent systems.[36] However, in cases where relatively large species are present, as with highly charged aggregates in our case, the straightforward grand-canonical approach becomes inefficient, because insertions/deletions of large particles are, then, to be done with the use of a gradual switching procedure[37,38] similar to that for polymers.[39] Therefore, we opted for a combined semi grand *NpT* ensemble, where the composition variations are achieved by use of the minimalist insertion-removal procedure with only small ionic species involved,[40] whereas the aggregate concentration is varied due to volume fluctuations. Note also that within the *NpT* framework, as long as $G_{NpT}^{(0)}(V)$ has been obtained for a given pressure, p_0, it is possible to find the coexistence pressure by numerically recalculating the profile as $G_{NpT}(V) = G_{NpT}^{(0)}(V) + (p - p_0)V$, and finding p^* that corresponds to equal depths of the two minima in $G_{NpT}(V)$[33,34] or, for a finite system, equal areas under the maxima in the probability distribution, $w(V;NpT) = \exp[-\beta G_{NpT}(V)]$.[41,42]

Thus, we performed our bulk simulations in an ensemble where temperature, T, external pressure, p, and number of aggregates, N_{agg}, were kept constant, while valency mutations between counterions were allowed. By performing a Legendre transformation of $\Xi(N_{agg},V,T,\Delta\mu_{ci})$, eq 8, into the semi grand Gibbs potential

$$G(N_{agg},p,T,\Delta\mu_{ci}) = \Xi(N_{agg},V,T,\Delta\mu_{ci}) + pV = \mu_{agg} N_{agg} = -k_B T \ln \mathcal{Q}(N_{agg},p,T,\Delta\mu_{ci})$$

(so that $dG = d\Xi + d(pV) = -S\,dT + V\,dp + \mu_{agg}\,dN_{agg}$), we arrive at

$$\mathcal{Q}(N_{agg},p,T,\Delta\mu_{ci}) = \int dV \exp[-\beta pV] \mathcal{Z}(N_{agg},V,T,\Delta\mu_{ci}) \quad (9)$$

Thus, the model Hamiltonian for this ensemble is

$$\mathcal{H}(N_{agg},p,T,\Delta\mu_{ci}) = \beta[U_{tot}(\mathbf{r}^N) - \Delta\tilde{\mu}_{ci} N_z + pV] - (N + 4/3) \ln V + \ln N_1! + \ln N_z! \quad (10)$$

Here the terms due to the relevant kinetic factors in eq 8 have been absorbed into the effective chemical potential difference, $\Delta\tilde{\mu}_{ci} = \Delta\mu_{ci} + k_B T \ln(q_z/q_1^z)$, $N_1 = |Z_{agg}|N_{agg} - |z|N_z$ as above, and the factor $(N + 4/3)$ corresponds to sampling of the *inverse* box length, $1/L$, rather than volume.[32] In practice, we have opted to measure distances in Å and, hence, the unit of q is Å^{-3}. Clearly, in eq 10 we skipped all the constant terms that do not affect sampling and, therefore, are irrelevant for the MC procedure.

As was mentioned above, to study a phase separation in such an ensemble, it is necessary to obtain $G_{NpT}(V)$ in a wide range of volumes. It is practically impossible, however, to sample in one simulation two phases that are separated by a free energy barrier significantly exceeding $k_B T$, unless some measures are taken to efficiently cross the barrier. With this in mind, we apply a self-consistent biasing procedure while sampling along the V-coordinate. As a result, we obtain a bias potential that represents a good estimate of the sought $G_{NpT}(V)$ function.

First, we modify the partition function so as to explicitly distinguish and reweight the semi grand canonical (sub)states,

$$\mathcal{Q}_{exp}(N_{agg},p,T,\Delta\mu_{ci}) = \int dV \exp[\beta\eta(V)] w_{NpT}(V) \quad (11)$$

where $\exp[\beta\eta(V)]$ is an arbitrary weighting function that will be chosen solely for the sake of convenience and efficiency of simulation, and

$$w_{NpT}(V) = \mathcal{Q}^{-1}(N_{agg},p,T,\Delta\mu_{ci}) \int dV'\ \delta(V' - V) \times \exp[-\beta pV'] \mathcal{Z}(N_{agg},V',T,\Delta\mu_{ci}) \quad (12)$$

In this form, $\mathcal{Q}_{exp}$ is identical to an expanded[43] semi grand canonical ensemble defined in a continuum domain of V. Obviously, the Hamiltonian in such an expanded ensemble includes a bias, so-called "penalty" or balancing, potential, $\eta(V)$,

$$\mathcal{H}_{exp}(N_{agg},p,T,\Delta\mu_{ci}) = \mathcal{H}(N_{agg},p,T,\Delta\mu_{ci}) + \eta(V) \quad (13)$$

The probability of encountering a particular volume while sampling in this ensemble is proportional to $\exp[\beta\eta(V)] w_{NpT}(V)$. Thus, if the weights are chosen such that $\exp[-\beta\eta(V)] \rightarrow w_{NpT}(V)$, then the sampling becomes uniform, and the balancing function $\eta(V) \rightarrow -k_B T \ln[w_{NpT}(V)] = G_{NpT}(V)$. It is not necessary, though, to know the latter in advance, before starting a simulation, because an estimate of it can be obtained in an iterative, self-consistent manner, so that when all the substates have been visited reasonably well, the final estimate is obtained as

$$G_{NpT}(V) \approx \eta(V) - k_B T \ln[w'_{NpT}(V)]\{+\text{const}\} \quad (14)$$

where $w'_{NpT}(V)$ is the actual probability distribution obtained with a given function $\eta(V)$.

Simulation Aspects. In the semi grand *NpT* ensemble the system should sample both coagulate and dilute phases in the course of the same simulation. In cases where counterion correlation effects are strong, complexes of two or more electrolyte aggregates can emerge even in the dilute regime. Also, at moderate to high electrolyte concentrations the multivalent counterions tend to adsorb onto the aggregate surface. All of these considerations represent challenges for generating a Monte Carlo trajectory that does not suffer from issues with ergodicity.

To enhance the conventional Metropolis sampling in configuration space, we adopted two global (cluster) MC steps that have been reported as efficient for asymmetric electrolytes.[46,47] A global translation move was applied for an aggregate together with the counterions found within some distance from its surface. We found that it is beneficial for convergence to choose this distance randomly between $R_{agg} + d$ and $1.3(R_{agg} + d)$. Then, to satisfy the principle of microreversibility, attempts resulting in a change of the number of counterions within the specified proximity range were rejected. Also, an inversion swap

of the content of spherical regions centered on two aggregates proved to be effective for improving statistics at moderate densities and in the dilute regime. Again, at each step the radius of the two spheres was chosen at random between $R_{agg} + d$ and $L/2$ (L being the box length). One of the two global moves was attempted in each MC sweep which also included one attempt on volume variation and two attempts on counterion mutation. The maximum displacement for each species was chosen so as to maintain the acceptance ratio close to 0.3; typical values would be $\Delta_{agg} = 0.1R_{agg}$, $\Delta_{mono} = L/2$, and $\Delta_{multi} = d...\ 2d$.

The mutation moves for counterions were implemented in the most straightforward fasion; i.e., no configurational bias was employed. First, a random selection was made as to which type of counterions (multivalent or monovalent) was to decrease in number. Then, either one multivalent ion or the corresponding number (2 or 3) of monovalent ions was (were) chosen at random, subject to removal. At the same time addition of the relevant number of complementary ions at random positions was also attempted, so as to maintain the system neutral. This way both the detailed balance principle and the electroneutrality condition were fulfilled, whereas the acceptance criteria for such ion mutation attempts were dictated by the Hamiltonian, eq 10.

As is easily understood, sampling a range of volumes sufficiently wide to reach both high and low densities in a single simulation is impractical. Therefore, we performed simulations in reasonably small subranges of volume, or V-windows, the width of which was gradually reduced as the aggregate concentration increased. That is, provided the same number of V-bins in a window, the discretization in V was denser for higher concentrations. In total, 5−10 windows were normally necessary, the number being dependent on how close the two sought phases were in terms of volume. To facilitate convergence in strongly coupled systems—mostly where trivalent counterions were present, we employed a replica-exchange scheme with subdivision of each V-window into 10 subwindows, similar to that reported in ref 44.

To obtain an estimate for $\eta(V)$ in eq 14, we applied an approach similar to the Wang−Landau (WL) scheme for the density of states,[45] with the following two differences. (i) In our case we obtain the density of substates in V-domain. (ii) After a preliminary simulation of WL-type (normally 3−5 WL-iterations) the self-consistent procedure for updating $\eta(V)$ was stopped, and a production run was carried out, often resulting in a rather uniform distribution of $w'_{NpT}(V)$ and, hence, accurate estimate of $G_{NpT}(V)$, eq 14. Normally we started with 250 000 MC sweeps per WL-iteration, in a window of 100 V-bins, and doubled the number of sweeps after each second iteration, which amounted to at least 1 000 000 sweeps during the production stage (∼10 000 per V-bin). In all the graphs presented below the statistical errors are within the size of symbols.

Results and Discussion

Polarizability of a Single Charged Colloid. To acquire understanding of the attractive forces between like-charged macro-aggregates, we start by considering a classical analogue of the quantum mechanical dispersion force. For two argon atoms this implies an attractive *induced dipole−induced dipole* interaction decaying with the atom separation as r^{-6}, which was first derived by London[30] within a quantum mechanical perturbation framework. This dispersion interaction cannot be described on the basis of purely classical arguments. It originates from the momentary correlations in movement of outer-shell electrons belonging to different atoms and actually explains why noble gas atoms condense.

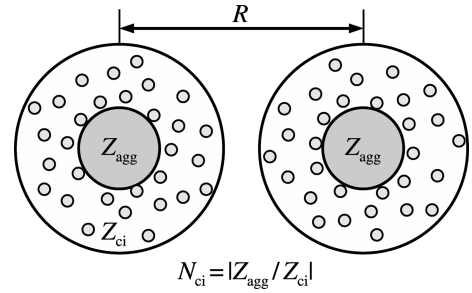

Figure 1. Sketch of the two-cell model for nonoverlapping spherical charge distributions around two macro-aggregates.

Now let us treat two nonoverlapping spherical charge distributions on classical grounds; see Figure 1. We can write the (excess) *free energy* of interaction, i.e., the work done upon bringing the two spherical cells, each comprising a charged aggregate with its counterions, from infinity to separation R,[48,49]

$$\beta\Delta A(R) = -\ln\langle\exp[-\beta\Delta U_{els}(\mathbf{r}^N,\mathbf{s}^N)]\rangle_0 \qquad (15)$$

where $\mathbf{r}^N$ represents the N (counter)ion coordinates in one spherical cell and $\mathbf{s}^N$ the coordinates in the other. For a given configuration of ions there is an interaction between the distributions which we denote $\Delta U(\mathbf{r}^N,\mathbf{s}^N)$. The brackets and subscript "0" symbolize a thermal average over the *noninteracting* (unperturbed) charge distributions; i.e., it suffices to simulate a single colloid with its counterions in a cell. For symmetry reasons the average $\langle\Delta U(\mathbf{r}^N,s^N)\rangle_0$ is trivially zero but the average $\langle\exp[-\beta\Delta U(\mathbf{r}^N,\mathbf{s}^N)]\rangle_0$ is *nonzero*.

Furthermore, the interaction energy $\Delta U(R)$, can be written as a two-center multipole expansion,[50] where the different terms represent charge−charge, charge−dipole, dipole−dipole interactions, etc. It is obvious from symmetry considerations that the two first terms vanish and that the first nonzero term is the dipole−dipole interaction. By expanding the logarithm in eq 15 and keeping only second-order terms in the interaction and including the first nonzero term in the multipole expansion, one obtains

$$\beta\Delta A \approx -\frac{3\alpha_1\alpha_2}{R^6} \qquad (16)$$

where α is the generalized polarizability for a cell defined as

$$\alpha = \left\langle\left(\sum_k Z_{ci} r_k\right)^2\right\rangle_0 \qquad (17)$$

The analogy between eq 16 and the quantum mechanical dispersion force is striking, whereas in the present case the α's have taken the place of atomic polarizabilities. The classical polarizability can be calculated with excellent accuracy in a simulation of a single cell. The so-obtained dependences of α on the counterion valency and the aggregate charge are shown in Figure 2. One can notice that the polarizability has a maximum, which happens to come at $Z_{ci} \approx 1$ for aqueous conditions. The position can be estimated by assuming that it is the "last" counterion that is the main contributor to α and that the maximum appears when it is "bound" by kT, that is

$$l_B\frac{Z_{ci}^2}{R_{agg}} = 1 \Rightarrow Z_{ci}^{max} \approx \sqrt{\frac{R_{agg}}{l_B}} \qquad (18)$$

The corresponding maximum in α is approximately equal to

$$\alpha_{max} \approx \frac{R_{agg} R_{cell}^{\ 2}}{l_B} \tag{19}$$

where $l_B = e^2/4\pi\epsilon_0\epsilon_r kT$. These estimates are in surprisingly good agreement with the simulated polarizabilities. In the extreme limit when $Z_{ci} = Z_{agg}$, then the polarizability becomes simply $\alpha = Z_{agg}^{\ 2} R_{agg}^{\ 2}$ and in the limit when $Z_{ci} \to 0$ then α goes to zero like $1/N_{ci}$.

A detailed comparison between the theoretical predictions and simulation results for this model can be found elsewhere.[50] Here our aim was to emphasize that purely thermal fluctuations within the unperturbed ionic atmosphere around a macro-ion give rise to a short-range attractive term in the total interaction between two ionic clouds. One can anticipate that allowing for charge redistribution in response to the interimposed field, i.e., both inter- and intracellular ionic correlations, should only make the effective induced-dipole attraction stronger. As a matter of fact, the attractive component captured by the second-order perturbational approach, eq 16, is relatively weak and cannot really compete with the strong long-range repulsion predicted by the Poisson−Boltzmann theory.[50] This repulsive (entropic) component has to be dealt with in a different manner. As we will see below, the major correlation effect, arising due to an increased counterion valency, is *not an increase of the short-range attractive term* discussed above, but *a decrease of the long-range repulsive one*.

Force between Two Charged Colloids. To illustrate different ion correlation regimes and the corresponding modulation effects on the *average net* force between two like-charged aggregates, we use MC simulations in a spherical cell for calculating the potential of mean force (POMF). The POMF is obtained by sampling the pair distribution function, $g_{agg}(R)$, for the two aggregates in a standard Metropolis simulation and we obtain

$$\beta A(R) = -\ln g_{agg}(R) \tag{20}$$

where R is the aggregate-aggregate separation; see Figure 3. This system is particularly suitable for spanning the relevant parameter space. Note that the radius of the outer (confining) sphere determines the aggregate concentration.

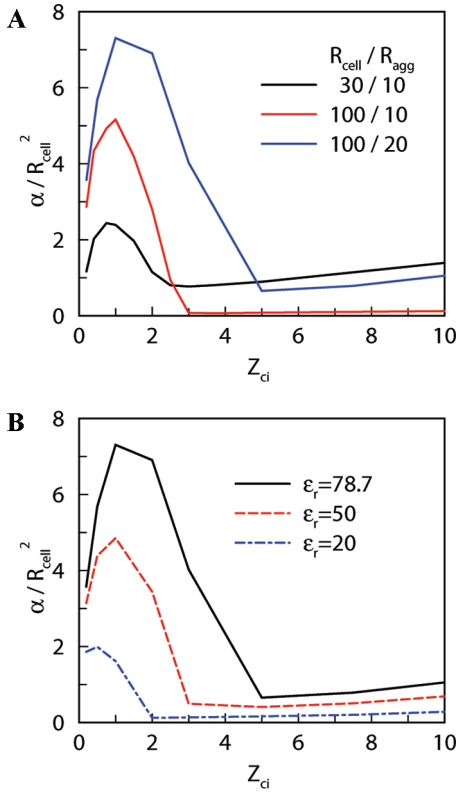

Figure 2. (A) Classical polarizability, α, as a function of the counterion valency for different cell and aggregate radii as indicated in the legend; $Z_{agg} = -30$ and $\epsilon_r = 78.7$. (B) Same as (A), but the dielectric permittivity is varied as indicated in the legend; $Z_{agg} = -30$, $R_{agg} = 20$ and $R_{cell} = 100$ Å.

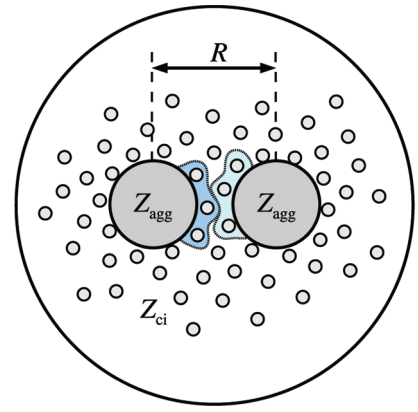

Figure 3. Sketch of the cell model with two like-charged aggregates and their counterions. Ionic correlations in the midregion are visualized by depicting the (momentary) areas of electrostatic exclusion (so-called "holes") around counterions in the vicinity of each aggregate (outlined and shaded).

How ion−ion correlations affect the interaction between two charged planar surfaces has been analyzed by Guldbrand et al.[17] and Attard et al.,[51,52] who showed that the coupling parameter determining the importance of ion correlations can be written as

$$\Gamma = \frac{Z_{ci}^{\ 4} l_B^{\ 2}}{h\lambda_{GC}} \qquad \lambda_{GC} = \frac{e}{2\pi|Z_{ci}|\sigma l_B} \tag{21}$$

with h being the surface separation, λ_{GC} the Gouy−Chapman length, and σ the surface charge density. The larger Γ, the more pronounced the deviation from the mean-field approximation, and ultimately, an attractive short-range minimum in the net pressure can emerge.

Equation 21 is valid for two infinite planes, whereas similar coupling parameters have been proposed for spherical macro-ions.[53,54] Although it may be possible to include the effects of the counterion adsorption density and the macro-ion curvature in a single coupling parameter, for a qualitative discussion it is instructive to consider the parameter,

$$\Gamma_S = \frac{l_B|Z_{ci}Z_{agg}|}{R_{agg} + R_{ci}} \tag{22}$$

which is essentially the electrostatic energy of a counterion at contact with a macro-ion and, as such, measures their coupling strength relative to the thermal energy (k_BT). Thus, large values of Γ_S indicate a regime of high counterion adsorption, which for $|Z_{ci}| > 1$ leads to strong correlation effects at short distances between two aggregates and, therefore, can result in a phase separation.

By comparing with eq 21, one can notice that Γ_S does not reflect the dependence on the aggregate separation. This is not crucial, though, because the ionic correlations responsible for the attractive force component manifest mostly at surface separations, $h = R - 2R_{agg}$, shorter than the so-called electrostatic exclusion "hole" of a counterion,[55−57] the diameter of

which can, in our case, be estimated roughly as $d_h = l_B Z_{ci}^2/3$, wherein the electrostatic repulsion between counterions exceeds 3 k_BT ($d_h \approx 2.4$, 9.5, and 21.4 Å for mono-, di-, and trivalent counterions, respectively, $T = 298$ K). Indeed, the mechanism of ionic correlations can be visualized by drawing the instantaneous picture of exclusion areas associated with counterions in the midregion, Figure 3. An alternative estimate for the attraction inset separation, proposed by Rouzina and Bloomfield[53] and later verified (for divalent counterions) by Lobaskin et al.,[58] is $d_s = (4\pi(R_{agg} + R_{ci})^2 Z_{ci}/Z_{agg})^{1/2}$, being the typical space between the adsorbed counterions, which gives approximately the same distance range. The simulation data show that the attraction range is rather narrow and does not vary significantly upon altering any of the parameters in eq 22. Thus, when considering the effects of varying concentration, which is important for prediction of phase stability, one should remember to compare the mean surface separation, $(h_S) = (\rho_{agg}^{-1/3} - 2R_{agg})$, with d_h (or $\rho_{agg}^{-1/3}$ vs d_s). One can also refer to eq 21 instead of eq 22.

We note that the effect of reduction in coupling due to an increased aggregate curvature can be incorporated in a simplified version of eq 21, $\Gamma(h) \propto l_B|Z_{ci}|\sigma/h$, by multiplying it by $S(R_{agg}) \approx \pi R_{agg}^2/9$, being an estimate of the (nearly flat) area exposed to the midregion. This results in $\Gamma(h) = l_B|Z_{ci}Z_{agg}|/(36h)$. Furthermore, to directly link the coupling strength to the attraction set-in separation, $\approx d_h$, one can replace l_B with the size of the electrostatic correlation hole, so as to obtain

$$\Gamma_h = \frac{d_h|Z_{ci}Z_{agg}|}{36h} = \frac{l_B|Z_{ci}^3 Z_{agg}|}{108(R - 2R_{agg})} \qquad (23)$$

One can see that $\Gamma_h^* \equiv \Gamma_h(d_h) = |Z_{ci}Z_{agg}|/36$ measures the coupling strength at separations close to where the (possible) attraction sets in. For instance, with $|Z_{agg}| = 30$ and $h = d_h$, eq 23 gives the following values in the cases of mono-, di-, and trivalent counterions: 0.8333, 1.666, and 2.5, respectively. The POMF data discussed below suggest that the condition of $\Gamma_h^* > 1$ can serve as a practical criterion for observing a notable minimum in POMF for $h < d_h$, whereas $\Gamma_h^* > 2$ appears to correlate well with the emergence of phase separation in our bulk simulations presented in the next section.

The effect of the counterion valency on POMF is demonstrated in Figure 4A. With monovalent ions the two charged spheres repel each other as the DLVO theory predicts, whereas already with divalent counterions there appears a weak minimum that becomes several k_BT's deep in the case of trivalent ions. This is the same type of behavior seen in many experimental studies. Here we emphasize that the crossover from repulsion to attraction in Figure 4A is mainly due to a reduced entropic repulsion. That is, the counterion cloud is less diffuse with di- or trivalent ions, which gives a weaker and shorter-ranged repulsion when the aggregates approach. The attractive component due to induced-dipoles, as described in Figure 2, though also being reduced, is less affected in relative terms, owing to the enhanced correlations between multivalent ions.

The electrostatic coupling can also be modulated via the Bjerrum length by changing temperature or dielectric permittivity. In the latter case, the easiest way is to consider a mixture of water and some other liquid of lower dielectric permittivity, e.g., alcohols like methanol or ethanol. Such mixtures will have progressively lower permittivity, when the amount of alcohol increases and the ion−ion correlation will become more important.[59] According to eq 22 there should also be dependency on the aggregate net charge, and the prediction is that the higher

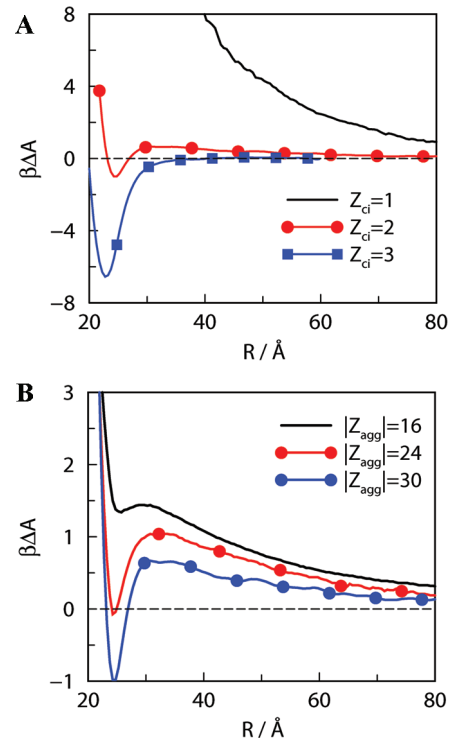

Figure 4. (A) Potential of mean force between two spherical aggregates with $Z_{agg} = -30$. The system contains no salt but only counterions of different valency and the cell radius is 100 Å. (B) Potential of mean force between two spherical aggregates of radius 10 Å for various aggregate charge. Only divalent counterions are present and $R_{cell} = 100$ Å.

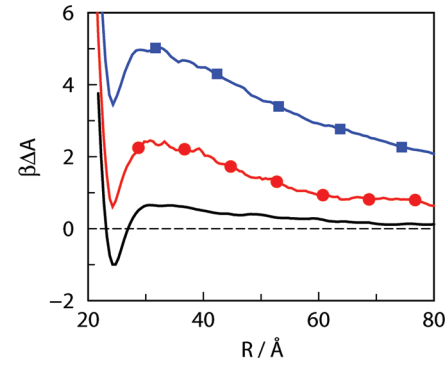

Figure 5. Potential of mean force between two spherical aggregates with $R_{agg} = 10$ Å, $Z_{agg} = -30$ and divalent counterions for varying cell radii; $R_{cell} = 100$ Å (black, no symbols), $R_{cell} = 200$ Å (red, spheres), and $R_{cell} = 400$ Å (blue, squares).

the charge of the aggregates the larger their attraction! This indeed born out in Figure 4B.

If we compare with the planar case, eq 21 indicates that the aggregate concentration also plays a role, which is illustrated in Figure 5. The potential of mean force is repulsive at low concentration, but it gradually turns into a net attraction at sufficiently high concentration. In fact, the dependence of effective potentials on aggregate concentration has been previously studied in detail by Lobaskin et al.[58] In their report the effective interaction within the Wigner−Seitz cell model with charge renormalization was tested against inversed Monte Carlo (IMC) data. Notably, already in the case of divalent counterions, both Poisson−Boltzmann solution and conventional Monte Carlo with charge renormalization failed to reproduce even qualitatively the attractive component in the effective pair potential. The IMC results gave, though, a clear indication of

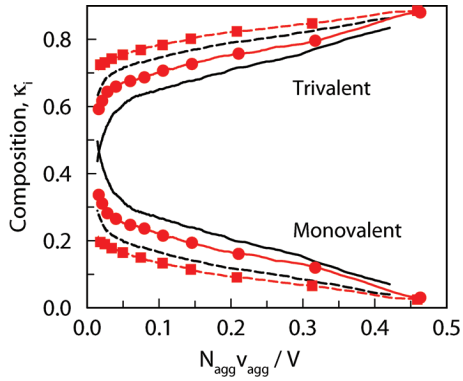

Figure 6. Composition of counterions as a function of aggregate volume fraction for systems with mono- and trivalent counterions present. Lines without symbols correspond to $Z_{agg} = -27$ and with symbols to $Z_{agg} = -30$. Solid lines are for $\beta\Delta\tilde{\mu}_{ci} = 12$ and dashed lines for $\beta\Delta\tilde{\mu}_{ci} = 14$.

short-range attraction, and our data presented in Figure 5 are in a good qualitative agreement with those. That is, the dependence on concentration is greatly pronounced in the drop of the repulsive long-range tail in the potential of mean force obtained at higher densities. At the same time, the minima responsible for attraction at short distances are affected by density variation only slightly, their depth being slowly reduced as the density is lowered. Of course, in the limit of infinite dilution the primary (attractive) minimum disappears.

Bulk Solution of Charged Macro-Aggregates. A comprehensive overview of different coupling regimes within the salt-free primitive model studied in extensive *NVT* simulations has been reported earlier by Linse,[54] where the corresponding bulk state points were also mapped onto a variety of experimental systems. However, in those simulations only "pure" phases, with mono-, di-, or trivalent counterions present, were considered, and all the evidence for possible phase separation was collected from indirect observations. In contrast, in this section we proceed to a bulk system consisting of aggregates neutralized by a mixture of *competing* mono- and multivalent counterions and also *directly* observe the crossover from supercritical phase behavior to phase coexistence. As suggested by eqs 21 and 22, the parameters of our model, such as d, R_{agg}, and Z_{agg}, are scalable; i.e., one can get the same coupling regime with different sets of parameters. Therefore, the physical phenomena observed with one set of parameters are, at least qualitatively, characteristic of all the systems with the same Γ_S. This guides our choice of rather small values of R_{agg} and Z_{agg} in comparison to systems studied previously.[27,28,47]

The molar fraction of the two counterion types is regulated by $\beta\Delta\tilde{\mu}_{ci}$. This is illustrated in Figure 6, where the composition for a mixture of mono- and trivalent counterions as a function of the aggregate volume fraction is given for different values of $\beta\Delta\tilde{\mu}_{ci}$. One can see that a higher value of $\beta\Delta\tilde{\mu}_{ci}$ gives a larger fraction of trivalent counterions. Figure 6 also shows how the fraction of trivalent counterions increases with increasing aggregate concentration. This is partly a trivial effect stemming from the ideal chemical potential; i.e., to keep $\beta\Delta\tilde{\mu}_{ci}$ constant, more monovalent ions must be replaced by trivalent as the density increases. For charged systems, the effect is more pronounced because trivalent ions are also energetically favored. The electrostatic coupling may also be enhanced by a higher aggregate charge promoting a higher fraction of trivalent ions in the solution; note the difference between black and red lines in Figure 6. A similar, albeit less dramatic, behavior is observed with a mix of mono- and divalent counterions (not shown). It

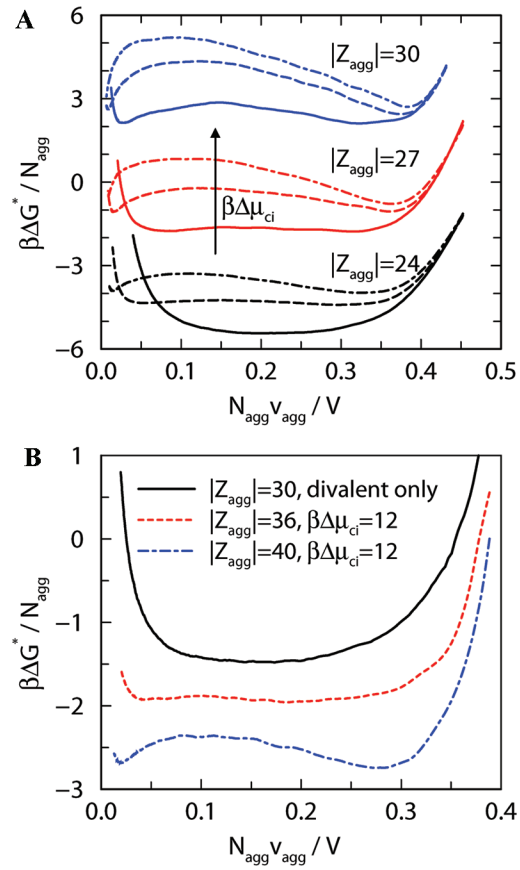

Figure 7. Constrained Gibbs free energy, eq 14, per aggregate for systems with mono- and trivalent (A) or divalent (B) counterions. The free energy is recalculated to pressures close to phase separation conditions. (A) The case of mono- and trivalent counterions. For each aggregate charge, Z_{agg}, three values of $\beta\Delta\tilde{\mu}_{ci} = 10$ (solid), 12 (dashed), and 14 (dot-dashed) are considered, so that the equilibrium is gradually shifted toward trivalent counterions. (B) Case of mono- and divalent counterions.

is worth noting that analogous partitioning of species in between charged surfaces is also found in a system with *only monovalnet* counterions where 1:1 salt is present.[60] Provided sufficiently high salt concentration (~0.4 M in the bulk), packing effects at the surfaces come into play and result in wavy modulations in the surface force. Furthermore, at even higher salt concentration (~2 M) the ion correlations within the electric double layer lead to emergence of an attractive (negative) minimum in the osmotic pressure at intermediate surface separations, which may in principle provoke a phase separation.[60]

In Figure 7A the constrained Gibbs free energy, eq 14, is presented for systems with a mix of mono- and trivalent counterions where the aggregate charge is varied, $|Z_{agg}| = 24$, 27, and 30. It is clear that, as the coupling strength and/or $\beta\Delta\tilde{\mu}_{ci}$ increase, so does the tendency to phase separate. To exemplify, $|Z_{agg}| = 24$ is certainly too low to promote a distinct phase separation at $\beta\Delta\tilde{\mu}_{ci} = 10$. The free energy profile is, however, rather "flat" for a range of intermediate densities, indicating a state close to a criticality. Increasing $\beta\Delta\tilde{\mu}_{ci}$ to 12 results in developing a barely distinguished bimodality in $G_{NpT}(V)$ which, at $\beta\Delta\tilde{\mu}_{ci} = 14$, transforms into a well pronounced barrier that separates the two coexisting phases: one with a high concentration of aggregates and the other at a much lower concentration. Strengthening the coupling in the system by increasing $|Z_{agg}|$ to 27 and 30, leads to emergence of two phases already at $\beta\Delta\tilde{\mu}_{ci} = 12$ and 10, respectively. The dense phase contains a substantially larger amount of trivalent ions and is stabilized

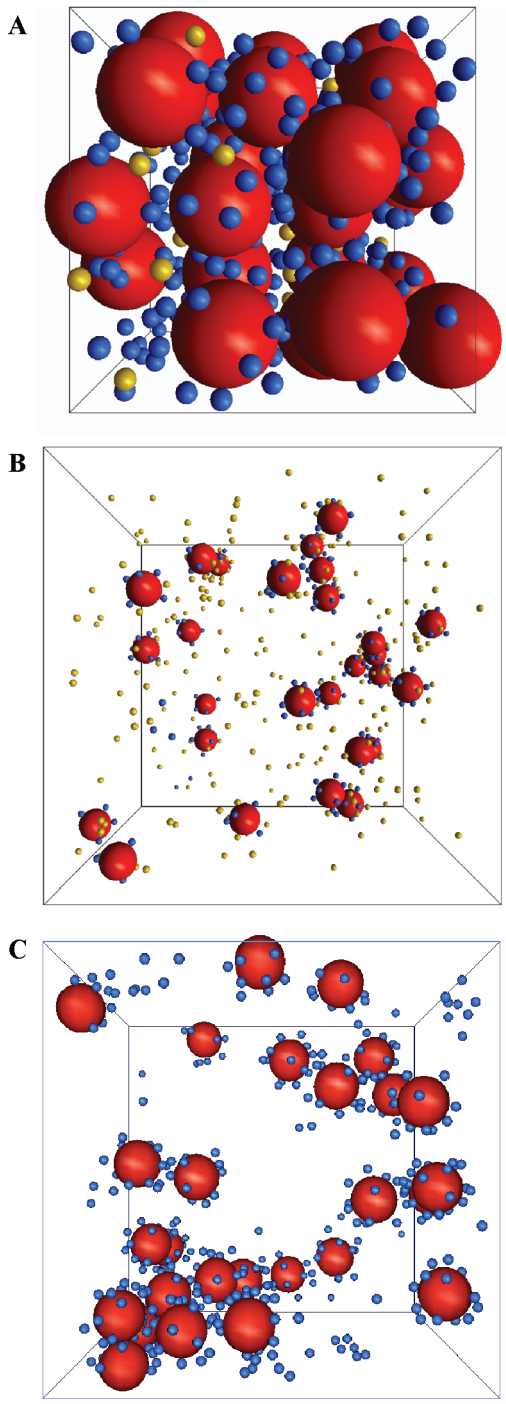

Figure 8. Simulation snapshots for systems with mono- and trivalent or only divalent counterions. Aggregates are red, monovalent ions are yellow (light), and multivalent ions are blue (dark), $|Z_{agg}| = 30$ in all cases. (A, B) Dense and dilute phases with mono- and trivalent ions. (C) Clustering in the system with only divalent ions; moderate density.

by strong electrostatic correlations, as discussed above. In contrast, the dilute phase benefits in entropic terms due to excess of monovalent ions. Thus, shifting the chemical equilibrium in the system toward trivalent counterions by raising $\beta\Delta\tilde{\mu}_{ci}$, makes the phase splitting in density progressively more pronounced. This is expected as the electrostatic coupling increases: the free energy of the dense phase is lowered due to stronger electrostatic correlations and to maintain equilibrium the density of the coexisting phase must be reduced compared to systems with lower $|Z_{agg}|$ or $\beta\Delta\tilde{\mu}_{ci}$.

Turning to systems where trivalent counterions have been replaced by divalent ones, we do not observe phase separation with the same aggregate charges even with only divalent ions present. The electrostatic coupling in all these cases appears to be insufficient, and the systems remain in states above the critical point. There are a few possibilities to provoke phase separation in these systems. Indeed, changing any of the quantities in eq 22 so that the coupling parameter, Γ_S, increases should do the work. For instance, by reducing temperature or dielectric permittivity one can make Bjerrum length longer and, hence, Γ_S larger, as we already discussed. The charge and radius of an aggregate are the other two parameters via which one can increase the coupling. Thus, if we increase $|Z_{agg}|$ above ~35, the phase coexistence picture is restored; see Figure 7B where we presented $G_{NpT}(V)$ profiles for $|Z_{agg}| = 30$, 36, and 40. It is worth mentioning that the limiting case of $R_{agg} \rightarrow \infty$, i.e., two charged planar surfaces with counterions in between, has been considered by Turesson et al.[40] who did actually obtain negative osmotic pressure with a mix of mono- and divalent counterions for a range of the surface charge densities corresponding to $|Z_{agg}|$ below 35 too. The discrepancy between our results should be attributed to different geometry of the coagulating aggregates. As one can see in Figures 4 and 5, the depth of the primary minima in the cases where we have divalent counterions is of the order $1 - 2k_BT$ only, and it varies only slightly with concentration. This implies that the curvature of the aggregate surface must be an important factor regulating the efficiency of ion correlations in between charged surfaces. That is, with small enough spherical aggregates (finite R_{agg}), such as in our case, the effective attraction at short distances is not sufficient to dominate over the thermal motion, owing to limitation of the midregion between aggregates where the attraction-inducting ion correlations take place (see Figure 3). Yet, *we do observe strong clustering* of aggregates even in relatively dilute solutions (see Figure 8), just as has been reported previously by Linse and Lobaskin. Altogether this is an important observation because intuitively one would expect phase separation whenever clustering between particles occurs, but we see that the actual phase behavior is more subtle than that. To summarize, in the case with divalent counterions there must be a crossover from supercritical phase behavior (mere clustering) to phase transition (coexisting phases) as R_{agg} grows.

Concluding Remarks

In this report we presented a theoretical analysis of the subtle interplay between repulsive and attractive forces arising between like-charged aggregates (be it colloids, micelles, or macro-ions) in the presence of counterions of different valencies. An account of the phenomena resulting from electrostatic correlation effects at the charged surfaces has been given within a simple and unified framework: starting with the classical polarization effects in the case of a single aggregate, then studying the effective pair interactions for two aggregates in various coupling regimes, and finishing by full chemical equilibrium Monte Carlo simulations of phase behavior in a bulk solution where mono- and multivalent ions are included explicitly and could exchange. Our analysis based on a single coupling parameter (for a particular geometry) as well as our simulation results suggests that a clear phase separation (coexistence) can be seen in suspensions with a sufficient amount of multivalent counterions present. Under certain conditions, however, when the electrostatic coupling due to ion correlations is not sufficiently strong, it is possible to observe aggregate clustering in a stable (semi)dilute phase, which resembles supercritical behavior in

simple fluids. We also found it instructive to compare our results for spherical aggregates with those obtained earlier for the case with planar surfaces and see how reducing the aggregate curvature can lead to a crossover between the supercritical and phase transition regimes.

Acknowledgment. Financial support by the Swedish Research Council (VR) through the Linnaeus Center of Excellence on Organizing Molecular Matter (OMM) and the Swedish Foundation for Strategic Research (SSF) is gratefully acknowledged. A.V.B. expresses his gratitude to Dr. A. Denton (Department of Physics, North Dakota State University) for valuable comments and suggestions on improvement of the original manuscript.

Note Added after ASAP Publication. This Article was published ASAP on April 15, 2009, with production errors in some equations (script Z's instead of italic Z's). In the text below eq 8, N_i and μ_i were changed to N_α and μ_α, and in the "Simulation Aspects" section, "20−50 windows" was changed to "5−10 windows". The corrected version was published on April 20, 2009.

References and Notes

(1) Gouy, G. *J. Phys. (Paris)* **1910**, *9*, 457.
(2) Chapman, D. L. *London Edinburgh Philos. Mag. J. Sci.* **1913**, *25*, 475.
(3) Derjaguin, B. V.; Landau, L. *Acta Phys. Chim. URSS* **1941**, *14*, 633.
(4) Verwey, E. J. W.; Overbeek, J. T. G. *Theory of the Stability of Lyophobic Colloids*; Elsevier Publishing Company Inc.: Amsterdam, 1948.
(5) Pashley, R. M. *J. Colloid Interface Sci.* **1981**, *83*, 531.
(6) Israelachvili, J. N.; Adams, G. E. *J. Chem. Soc., Faraday Trans. I* **1978**, *74*, 975.
(7) Shubin, V. E.; Kekicheff, P. *J. Colloid Interface Sci.* **1993**, *155*, 108.
(8) Khan, A.; Fontell, K.; Lindman, B. *J. Colloid Interface Sci.* **1984)** , *101*, 193.
(9) Khan, A.; Fontell, K.; Lindman, B. *Colloids Surf.* **1984**, *11*, 401.
(10) Marra, J. *Biophys. J.* **1986**, *50*, 815.
(11) Shaw, D. J. *Introduction to Colloid and Surface Chemistry*, 4th ed.; Butterworths: London, 1992.
(12) Kjellander, R.; Marčelja, S.; Pashley, R. M.; Quirk, J. P. *J. Chem. Phys.* **1990**, *92*, 4399.
(13) Gosule, L. C.; Schellman, J. A. *Nature (London)* **1976**, *259*, 333.
(14) Wilson, R. W.; Bloomfield, V. A. *Biophys. Chem.* **1979**, *18*, 2192.
(15) Mel'nikov, S. M.; Sergeyev, V. G.; Yoshikawa, K. *J. Am. Chem. Soc.* **1995**, *117*, 2401.
(16) Plassard, C.; Lesniewska, E.; Pochard, I.; Nonat, A. *Langmuir* **2005**, *21*, 7263.
(17) Guldbrand, L.; Jönsson, B.; Wennerström, H.; Linse, P. *J. Chem. Phys.* **1984**, *80*, 2221.
(18) Kjellander, R.; Marčelja, S. *Chem. Phys. Lett.* **1984**, *112*, 49.
(19) Kjellander, R.; Marčelja, S. *J. Chem. Phys.* **1985**, *82*, 2122.
(20) Forsman, J. *J. Phys. Chem. B* **2004**, *108*, 9236.
(21) Sogami, I.; Ise, N. *J. Chem. Phys.* **1984**, *81*, 6320.
(22) Ise, N.; Ito, K.; Okubo, T.; Dosho, S.; Sogami, I. *J. Am, Chem. Soc.* **1985**, *107*, 8074.
(23) Tata, B. V. R.; Ise, N. *Phys. Rev. E* **2000**, *61*, 983.
(24) Overbeek, J. G. *J. Chem. Phys.* **1987**, *87*, 4406.
(25) Woodward, C. E. *J. Chem. Phys.* **1988**, *89*, 5140.
(26) Linse, P.; Jönsson, B. *J. Chem. Phys.* **1983**, *78*, 3167.
(27) Linse, P.; Lobaskin, V. *Phys. Rev. Lett.* **1999**, *83*, 4208.
(28) Linse, P. *J. Chem. Phys.* **2000**, *113*, 4359.
(29) Linse, P. *Adv. Polym. Sci.* **2005**, *185*, 111.
(30) London, F. *Z. Phys. Chem. (B)* **1930**, *11*, 222.
(31) Metropolis, N. A.; Rosenbluth, A. W.; Rosenbluth, M. N.; Teller, A.; Teller, E. *J. Chem. Phys.* **1953**, *21*, 1087.
(32) Frenkel, D.; Smit, B. *Understanding Molecular Simulation*; Academic Press: San Diego, 1996.
(33) Hunter, J. E.; Reinhardt, W. P. *J. Chem. Phys.* **1995**, *103*, 8627.
(34) Broukhno, A. V. Free Energy and Surface Forces in Polymer Systems. Ph.D. Thesis, Lund University, Sweden, 2003.
(35) Panagiotopoulos, A. Z. *J. Phys.: Condens. Matter* **2000**, *12*, 25.
(36) Panagiotopoulos, A. Z. *Mol. Phys.* **1987**, *61*, 831.
(37) Borówko, M.; Zagórski, R.; Malijevský, A. *J. Chem. Phys.* **2000**, *112*, 2315.
(38) Vrabec, J.; Kettler, M.; Hasse, H. *Chem. Phys. Lett.* **2002**, *356*, 431.
(39) Wilding, N. B.; Müller, M. *J. Chem. Phys.* **1994**, *101*, 4324.
(40) Turesson, M.; Forsman, J.; Åkesson, T.; Jönsson, B. *Langmuir* **2004**, *20*, 5123.
(41) Borgs, C.; Kotecký, R. *Phys. Rev. Lett.* **1992**, *68*, 1734.
(42) Wilding, N. B.; Binder, K. *Physica A* **1996**, *231*, 439.
(43) Lyubartsev, A.; Martsinovski, A. A.; Shevkunov, S. V.; Vorontsov-Velyaminov, P. N. *J. Chem. Phys.* **1992**, *96*, 1776.
(44) Brukhno, A. V.; Anwar, J.; Davidchack, R.; Handel, R. *J. Phys.: Condens. Matter* **2008**, *20* (49), 494243.
(45) Wang, F.; Landau, D. P. *Phys. Rev. E* **2001**, *64*, 56101.
(46) Linse, P.; Lobaskin, V. *J. Chem. Phys.* **2000**, *112*, 3917.
(47) Lobaskin, V.; Qamhieh, K. *J. Phys. Chem. B* **2003**, *107*, 8022.
(48) Zwanzig, R. W. *J. Chem. Phys.* **1954**, *22*, 1420.
(49) McQuarrie, D. A. *Statistical Mechanics*; Harper Collins: New York, 1976.
(50) Woodward, C. E.; Jönsson, B.; Åkesson, T. *J. Chem. Phys.* **1988**, *89*, 5145.
(51) Attard, P.; Kjellander, R.; Mitchell, D. J.; Jönsson, B. *J. Chem. Phys.* **1988**, *89*, 1664.
(52) Attard, P.; Mitchell, D. J.; Ninham, B. W. *J. Chem. Phys.* **1988**, *88*, 4987.
(53) Rouzina, I.; Bloomfield, V. A. *J. Phys. Chem.* **1996**, *100*, 9977.
(54) Linse, P. *Philos. Trans. R. Soc. London A* **2001**, *359*, 853.
(55) Nordholm, S. *Chem. Phys. Lett.* **1984**, *105*, 302.
(56) Penfold, R.; Nordholm, S.; Nichols, N. *J. Stat. Mech.: Theory Exp.* **2005**, P06009.
(57) Penfold, R.; Jönsson, B.; Robins, M. *J. Stat. Mech.: Theory Exp.* **2005**, P06010.
(58) Lobaskin, V.; Qamhieh, K. *Phys. Rev. E* **2001**, *63*, 020401.
(59) Mel'nikov, S. M.; Khan, M. O.; Lindman, B.; Jönsson, B. *J. Am. Chem. Soc.* **1999**, *121*, 1130.
(60) Åkesson, T.; Jönsson, B. *Electrochim. Acta* **1991**, *36*, 1723.

JP811147V